Chem



Article

Macrocyclic ligand-driven ion selectivity and high surface area in a 2D conductive MOF



This work presents a novel two-dimensional electrically conductive metal-organic framework (2D EC-MOF), denoted as Cu-EP. The MOF was constructed using a macrocyclic ligand (EP), which was rationally designed from phenanthrene and ethynyl moieties. Through the design, we integrated large intrinsic pockets within a conductive framework. These pockets not only augment Cu-EP's surface area to a record high for 2D EC-MOFs but confer an additional layer of functionality, demonstrating ion selectivity.

Hoai T.B. Pham, Ji Yong Choi, Xiaoyu Fang, ..., Lacey Wayment, Wei Zhang, Jihye Park

jihye.park@colorado.edu

Highlights

Synthesis of a macrocyclic ligandbased 2D conductive metalorganic framework

Integrating large intrinsic pockets for complementary surface area

Intrinsic pocket-driven ion selectivity for Cs over Li ions

Advantageous redox activity in capacitive performance

7 AFFORDABLE AND CLEAN ENERGY

Pham et al., Chem 10, 199–210 January 11, 2024 © 2023 Elsevier Inc. https://doi.org/10.1016/j.chempr.2023.08.026



Chem



Article

Macrocyclic ligand-driven ion selectivity and high surface area in a 2D conductive MOF

Hoai T.B. Pham,¹ Ji Yong Choi,¹ Xiaoyu Fang,¹ Adam Claman,¹ Shaofeng Huang,¹ Samuel Coates,¹ Lacey Wayment,¹ Wei Zhang,^{1,2} and Jihye Park^{1,2,3,*}

SUMMARY

Two-dimensional electrically conductive metal-organic frameworks (2D EC-MOFs) have emerged as promising electronic materials despite their low surface areas and limited functionalities. Herein, we exploited molecular-level design of a macrocyclic ligand, ethynylphenanthrene (EP), wherein intrinsic pockets target both complementary surface area and extra layer of functionality. With copper nodes, Cu-EP exhibits an electrical conductivity of 1.0×10^{-3} S/cm and a record-high surface area of 1,502 m²/g among reported 2D EC-MOFs. Moreover, the intended large intrinsic pocket (6.5 Å) demonstrates capability to host bulky electrolytes, enhancing capacitive performance. Additionally, the pockets of Cu-EP selectively host Cs⁺ over Li⁺. Our results boast rational design of large intrinsic pockets to address common limitations of 2D EC-MOFs and further contribute to diversifying their functions with redox activity and ion selectivity, promoting a new paradigm for EC-MOFs' broader utilities.

INTRODUCTION

Two-dimensional electrically conductive metal-organic frameworks (2D EC-MOFs) have received growing attention due to their capability to transport electrons in a porous platform. This unique feature has enabled their utilization in energy storage, sensing, and electrocatalysis. 1–5 Unlike conventional MOFs, however, most 2D EC-MOFs often suffer from low surface areas, discouraging their maximal performance in such applications. We anticipate that 2D EC-MOFs with high surface areas could provide an extra layer of functionality, unlocking their fullest potential.

Improving the surface areas or integrating functionalities into 2D EC-MOFs has been challenging due to the limited ligand motifs and their synthetic difficulties associated with achieving the respective d-p conjugation.⁶ To tackle this issue, we set our underpinning ligand design criteria by first surveying ligands that have been previously employed for constructing 2D EC-MOFs and their respective MOFs' theoretical surface areas reported in the literature (Figure 1A).⁷ These theoretical surface areas may not directly correspond to experimentally obtainable values due to other factors such as crystallinity, crystal size, and stacking modes.⁷ However, they can guide the maximum surface areas that the respective EC-MOFs can achieve. Thus, they provide valuable insights into the relationship between the structures of ligands and their properties. Among the 3-fold symmetry containing ligands, the ligand size from benzene (B) to triphenylene (TP) and truxene (TX) could augment the theoretical Brunauer-Emmett-Teller (BET) surface areas from 633, 1,201, and 1,547 m²/g,

THE BIGGER PICTURE

The convergence of electrical conductivity and porosity in twodimensional electrically conductive metal-organic frameworks (2D EC-MOFs) positions them as up-and-coming materials for energy storage, sensing, electrocatalysis, and electronic applications. However, most 2D EC-MOFs suffer from low surface areas while presenting a scarcity of functionality. This work undertakes a strategic design to synthesize a macrocyclic ligandbased EC-MOF, denoted as Cu-EP, featuring large intrinsic pockets to surmount these limitations. Remarkably, Cu-EP showcases unprecedented surface area, surpassing most existing 2D EC-MOFs. Moreover, Cu-EP demonstrates ion selectivity for Cs over Li ions, concurrently exhibiting pronounced redox activity. We believe our work addresses prevalent challenges within the realm of conductive 2D MOFs and propels the boundaries of 2D EC-MOFs' potential to broader horizons.



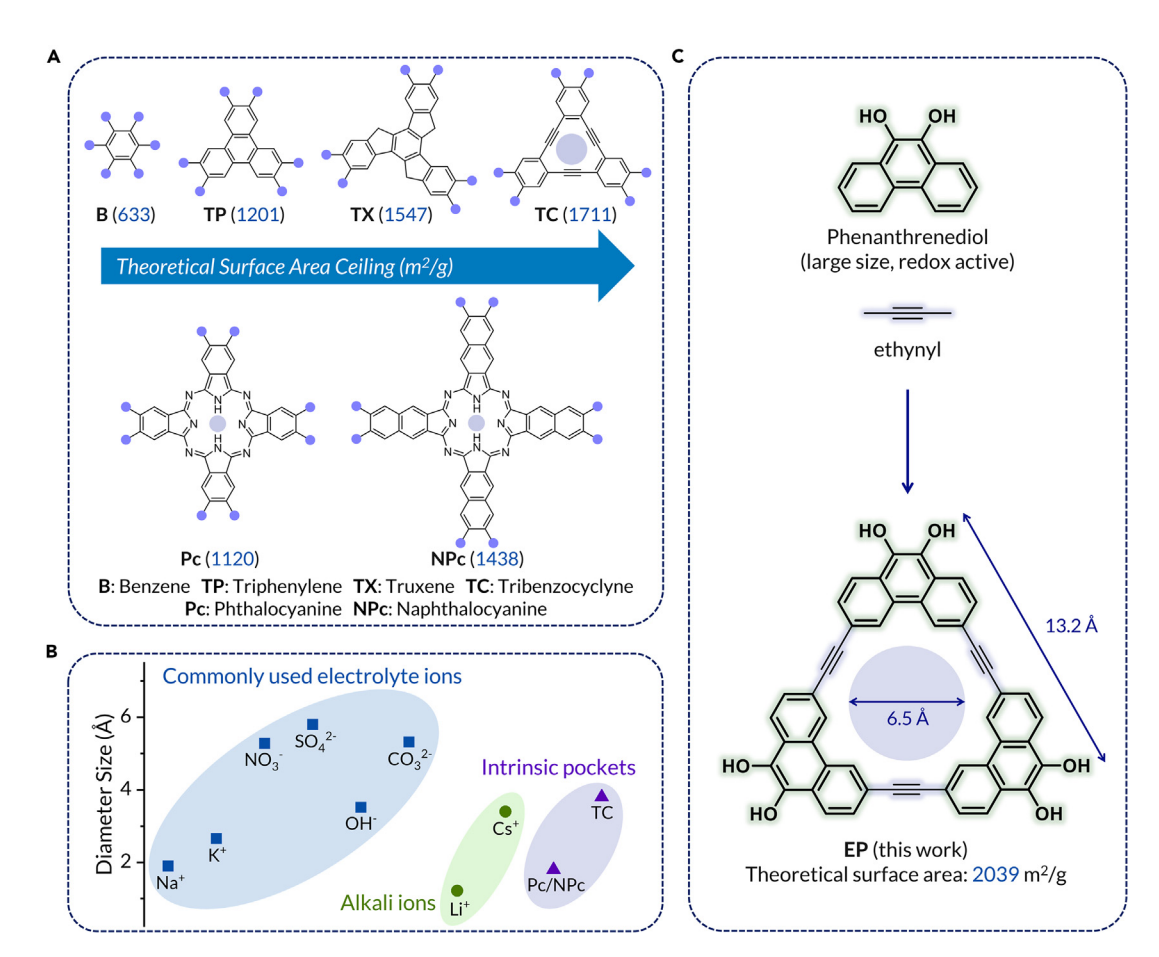


Figure 1. Strategic design of EP ligand

(A) Examples of ligand motifs for constructing 2D EC-MOFs and respective MOFs' theoretical surface area ceilings in parentheses adopted from the literature. Circles highlighted in light purple represent intrinsic pockets of the ligands.

- (B) Size comparison of commonly used electrolyte ions, alkali ions, and intrinsic pockets of reported ligands.
- (C) Synthetic scheme of the EP ligand from organic building blocks.

respectively. This finding is also consistent with the ligands with 4-fold symmetry as the theoretical BET surface area increases from 1,120 to 1,438 m²/g when naphthalocyanine (NPc) replaces phthalocyanine (Pc) cores. Interestingly, despite having a comparable core size of TX with tribenzocyclyne (TC), TC exhibits a higher theoretical surface area likely due to the contribution of its intrinsic pocket. With this in mind, we targeted a ligand with a large intrinsic pocket, ethynylphenanthrene (EP), to take the lead as 2D EC-MOFs with high surface areas.

Besides achieving an expected contribution of a higher surface area from a larger intrinsic pocket, we also exploited it to integrate functionalities because the pockets of TC, Pc, and NPc could impart a layer of functionality, such as metalation by providing binding affinity to transition metals. However, their relatively small pockets may limit hosting large ions, such as Cs, with an ionic size of $\sim\!\!3.5$ Å (Figure 1B). We envisioned that a larger intrinsic pocket (>6.0 Å) would be able to host Cs ion into the framework, potentially opening the door to Cs's appealing properties in catalysis and photovoltaics. Additionally, the large pocket can accommodate bulky guests, like commonly used aqueous electrolytes (from 2 to 6 Å), Potentially maximizing capacitive performance in energy storage.

¹Department of Chemistry, University of Colorado Boulder, Boulder, CO 80309, USA

²Materials Science & Engineering Program, University of Colorado Boulder, Boulder, CO 80303, USA

³Lead contact

^{*}Correspondence: jihye.park@colorado.edu https://doi.org/10.1016/j.chempr.2023.08.026





Based on the above design rationales, we synthesized a macrocyclic ligand EP via Mo-catalyzed alkyne metathesis from the monomer building blocks containing phenanthrenediol and ethynyl units (Figure 1C). We targeted the ethynyl moiety because the alkyne group can chelate a metal ion, enabling post-synthetic modification with binding affinity provided by the π electrons. According to our simulation (see supplemental information for details), the phenanthrenediol building block could theoretically lead to an unprecedentedly high theoretical surface area of 2,039 m^2/g , due to its large size (~13.2 Å) and the pocket size (~6.5 Å) (Figure 1C). In addition, phenanthrene derivatives are known for significant redox activity, 14 which may enable a wide range of functional properties, such as electrochromism, molecular electronics, and electrochemical energy storage. $^{15-17}$

Herein, we present a 2D EC-MOF, featuring EP as the coordinating ligand and copper as the node. The $Cu_3(EP)_2$, namely Cu-EP, exhibits an electrical conductivity of 1.0×10^{-3} S/cm and one of the highest surface areas of $1,502 \, \text{m}^2/\text{g}$ among reported 2D EC-MOFs. We demonstrated that the high surface area, pronounced redox activity, and ion selectivity of Cu-EP attributed to the ligand design containing a large intrinsic pocket. In particular, Cu-EP realizes ion selectivity for cesium over lithium, exploiting the large ethynyl pockets.

RESULTS AND DISCUSSION

Synthesis and optimization of Cu-EP

EP ligand could be synthesized by Pd(0)/Cu(I)-catalyzed cross-coupling of ethynyl bromophenanthrene derivatives, but this synthetic method often yields low with undesirable oligomers. $^{18-20}$ Thus, we pursued reversible alkyne metathesis instead for selective cyclotrimerization with a high yield. However, the reported method employing t-butyldimethylsilyl (TBDMS) ether-protecting group remains challenging to purify. 21 To accomplish a reliable ligand synthesis, we modified the present alkyne metathesis method to use ethylene glycol as an acetal-protecting group, making it practically more useful for MOF synthesis with a high yield of overall $\sim\!51\%$ (see supplemental information for detailed synthesis).

Cu-EP was synthesized via solvothermal synthesis, where copper(II) nitrate reacts with EP ligands in N,N-dimethylformamide (DMF) (Figure 2A). We initially screened typical kinetic parameters, including temperatures, concentrations, and reaction time to obtain highly crystalline Cu-EP (Figures S13-S15). To our surprise, we discovered that varied volumes of water could substantially alter crystallinity. As water volume increased from 0.2 to 0.4 mL to a 10 mL DMF used for each batch, the crystallinity of Cu-EP significantly improved (Figure S16). However, adding a higher volume of water (>0.6 mL for 10 mL DMF) rather reduced the crystallinity. Inspired by the water's impacts that we observed, we investigated its role in MOF synthesis. We calculated the pK_a of EP ligand and molecular water in DMF environments using density functional theory (DFT) (Table S1). Our calculations show that pK_a(1) and pK_a(2) of the EP ligand are much lower than the pK_a of water in DMF (Table S2). The pK_a trends of phenol derivatives and molecular water found here are consistent with relevant work conducted in nonaqueous environments.^{22,23} These calculations corroborate the ability of water to deprotonate the ligands, suggesting that water is a base for the synthesis of Cu-EP.

Structure characterization of Cu-EP

To elucidate the structure of Cu-EP, we collected powder X-ray diffraction (PXRD) patterns of the MOF. We fitted it against the simulated AA eclipsed, AB staggered, and AA slipped-parallel packing models, where the AA slipped-parallel packing

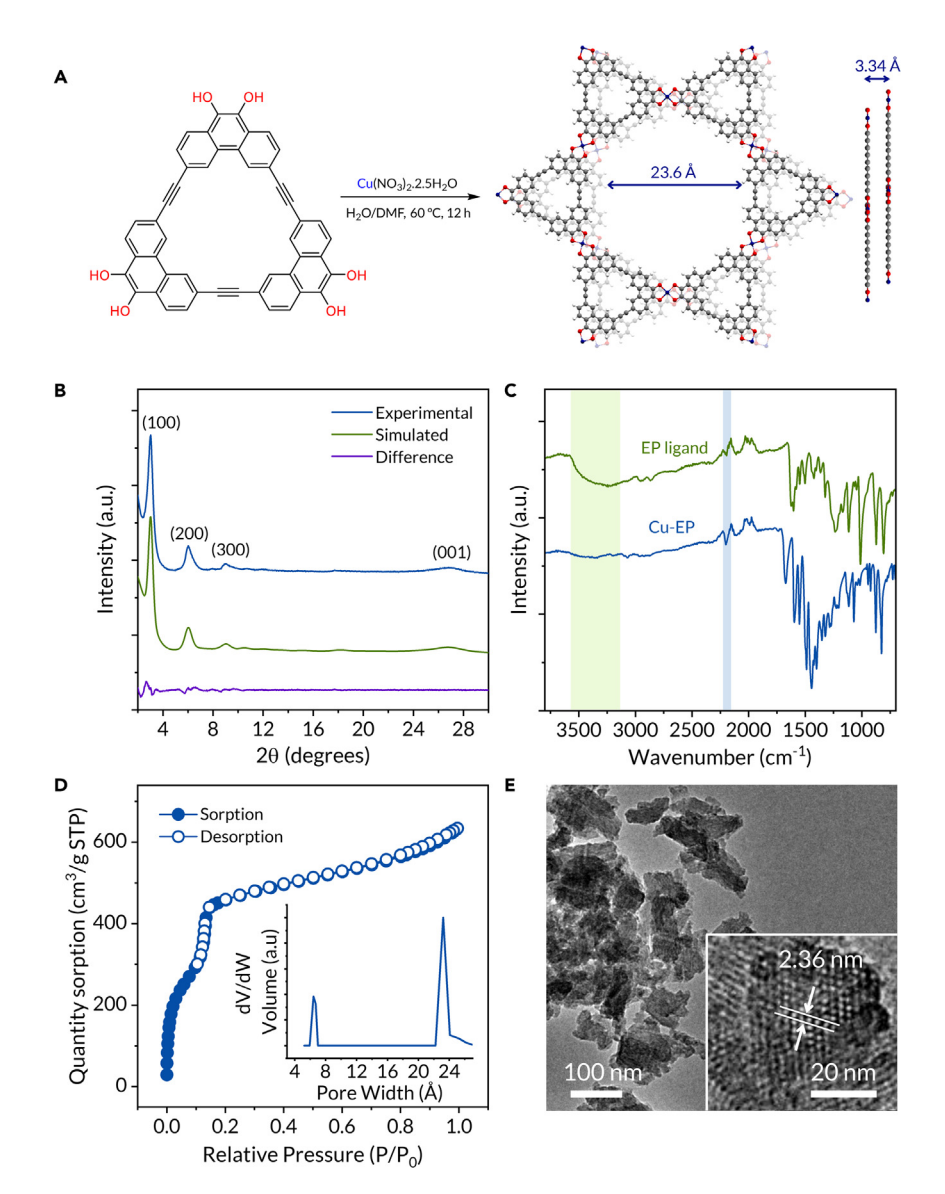


Figure 2. Synthesis and characterization of Cu-EP

- (A) Synthesis of Cu-EP and its simulated AA-slipped stacking mode.
- (B) Comparison of experimental and simulated PXRD of Cu-EP.
- (C) FTIR spectra of the EP ligand and Cu-EP. The highlights in green and blue represent the O–H and $C \equiv C$ vibrations, respectively.
- (D) Argon sorption isotherm (inset: pore width distribution) of Cu-EP.
- (E) TEM image of Cu-EP along with a lattice distance. Scale bars represent 100 nm (main) and 20 nm (inset).

provided the best fit to the experimental diffractions (Figure S18). The experimental PXRD patterns of Cu-EP were refined against Pawley fit, showing a good agreement with R_w of 5.13% (Figure 2B). Cu-EP represents a unit cell with the hexagonal space group of P6/mmm, and the lattice parameters of a = b = 33.95 Å and c = 3.34 Å (Table S3).

Fourier transform infrared (FTIR) spectroscopy of Cu-EP shows the disappearance of the O–H stretching vibration (3,200–3,600 cm⁻¹) after the reaction, confirming the coordination (Figure 2C). Both ligand and Cu-EP FTIR spectra display absorption



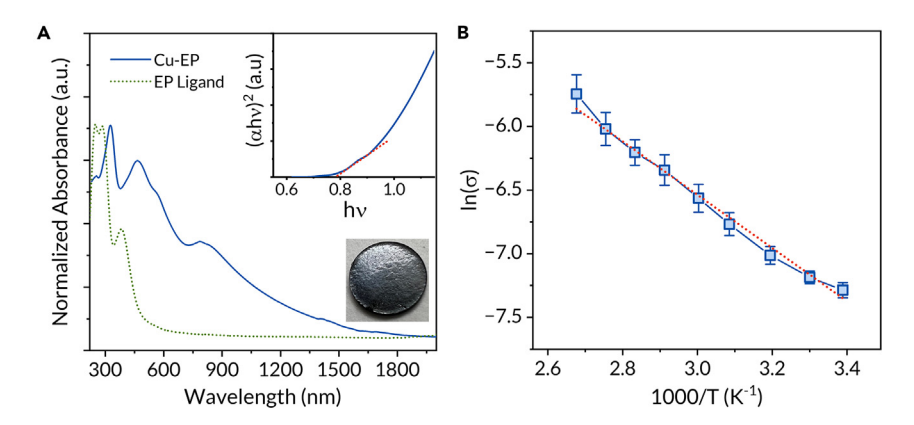


Figure 3. Electronic structure characterization of Cu-EP

(A) UV-vis-NIR spectra of the EP ligand and Cu-EP (inset: its Tauc plot and pellet).

(B) Electrical conductivity of Cu-EP under vacuum with varying temperatures. Error bars represent standard deviation of temperature-dependent electrical conductivity.

at around 2,230 cm $^{-1}$, showing a characteristic C \equiv C stretching vibration, which confirms that the alkyne functional group in the ligand remains intact after the MOF synthesis.

Then, the porosity and the surface area were investigated by argon sorption isotherm at 77 K (Figure 2D). As we rationalized, the material shows an unprecedentedly high BET surface area of 1,502 m²/g, of which the value surpasses most reported 2D EC-MOFs' (Figure S20; Table S4). $^{2,8,24-30}$ This record-high surface area must stem from the targeted ligand size, the extra contribution of large intrinsic pockets, as well as excellent crystallinity. 7,24 The non-local DFT (NL-DFT)-calculated pore width distribution shows two dominant pore widths of around 6.5 and 23.5 Å at maxima. The smaller pore of 6.5 Å can be ascribed to the intrinsic ligand pocket, suggesting the successful integration of pockets into the framework, which also agrees with our simulated AA slipped-stacking model.

X-ray photoelectron spectroscopy (XPS) scan of Cu(2p) suggests the presence of both Cu(I) and Cu(II) species in the MOF (932.3 and 934.2 eV at the $2p_{3/2}$ level, respectively), which coincide with other Cu-based 2D EC-MOFs (Figure S21), whereas Cu(II) being dominant with strong characteristic satellite peaks. ^{2,8,31} The deconvoluted O(1s) scan shows two distinguishable binding energies at 530.9 and 532.3 eV, which can be ascribed to C=O and C-O, respectively (Figure S21), ² suggesting the characteristic [CuO₄] coordination in 2D EC-MOFs. The scanning electron microscopy (SEM) and transmission electron microscopy (TEM) images of Cu-EP show aggregated nanocrystallites (<100 nm) (Figures 2E and S22). TEM analysis along the [001] direction revealed a lattice distance of 2.36 nm, which is in good agreement with the simulated model and the pore size distribution.

Electronic structure characterization

Ultraviolet-visible-near infrared (UV-vis-NIR) spectroscopy of Cu-EP exhibits a new absorption at 800 nm extending to the near-infrared region, which is absent in the free EP ligand, indicating an effective d- π conjugation between the metal node and EP ligand (Figure 3A). The Tauc plot derived from the absorbance spectrum determined an optical band gap of 0.8 eV. The bulk electrical conductivity was measured on a pressed pellet via the four-point probe method under ambient conditions. Cu-EP exhibits an electrical conductivity of 1.0 \times 10⁻³ S/cm, comparable





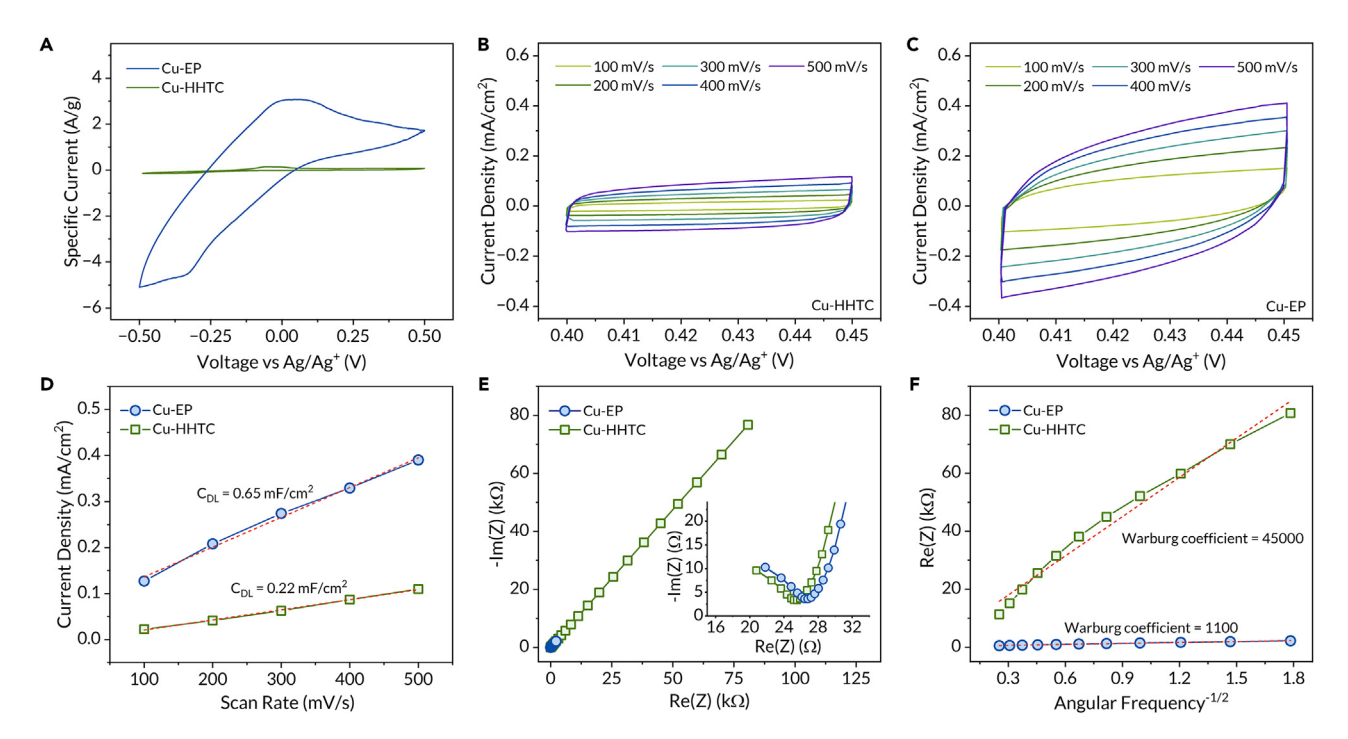


Figure 4. Electrochemical characterization of Cu-EP

- (A) Cyclic voltammetry of Cu-HHTC and Cu-EP in 1 M Na₂CO₃ with a scan rate of 10 mV/s.
- (B) Scan rate dependence of current density of Cu-HHTC in 1 M Na₂CO₃.
- (C) Scan rate dependence of current density of Cu-EP in 1 M Na₂CO₃.
- (D) Electrochemical double-layer capacitance analysis of Cu-HHTC and Cu-EP.
- (E) Electrochemical impedance spectra of Cu-HHTC and Cu-EP at frequencies between 1 MHz and 50 mHz in 1 M Na₂CO₃.
- (F) Angular frequency dependence of Warburg impedance.

with most EC-MOFs featuring [CuO₄] coordination (Figure S20; Table S4).^{8,26} By fitting the conductivity as a function of temperature (293–363 K) to the Arrhenius equation, $\sigma = \sigma_0 \exp(-E_a/k_BT)$, where σ_0 is a pre-factor, E_a is the thermal activation energy, k_B is Boltzmann constant, and T is the absolute temperature, the activation energy was calculated to be 0.2 eV (Figure 3B).

Electrochemical properties

To demonstrate the importance of the high surface area, large intrinsic pocket, and built-in redox features of Cu-EP, we first performed cyclic voltammetry (CV) to investigate its electrochemical properties in commonly used aqueous electrolyte systems (Figures 4A and S24). We also conducted a control experiment on Cu-HHTC (HHTC: 2,3,8,9,14,15-hexahydroxyltribenzocyclyne), an analogous EC-MOF constructed from a TC derivative, which showed a comparable conductivity yet a lower surface area and smaller intrinsic pockets. Compared with Cu-HHTC, Cu-EP shows more notable electrochemical features as follows: (1) more pronounced redox peaks and (2) much higher capacitance. Notably, the difference in capacitance between these two MOFs is more pronounced by 35-fold when 1 M Na₂CO₃ was used as the electrolyte (Figure 4A; Table S5), and we used the Na₂CO₃ electrolyte conditions for further electrochemical characterization.

We measured current density with varied scan rates from 100 to 500 mV/s in the $0.40-0.45\,\mathrm{V}$ (versus $\mathrm{Ag/Ag}^+$) window, where redox features are negligible. As shown in Figures 4B and 4C, the current density of Cu-EP is higher than that of Cu-HHTC at





the same scan rate. As a result, the capacitance of Cu-EP in this non-faradaic window is estimated to be about $3\times$ higher than that of Cu-HHTC (Figure 4D), which could be correlated to their different surface areas, ^{8,32} highlighting the importance of surface area in electrochemical storage. Nonetheless, this 3 times improvement of nonfaradaic capacitance is marginal to account for the observed 35-fold increase in capacitive performance, suggesting a significant faradaic charge-storage contribution from redox reactions. Further investigation into Cu-EP redox behaviors reveals an extra reduction peak at -0.3 V (versus Ag/Ag⁺) unlike Cu-HHTC, corroborating the additional redox activity of Cu-EP. Moreover, Cu-EP has a larger channel width than Cu-HHTC, ⁸ suggesting different electrolyte diffusion rates for the two systems. Additionally, the small intrinsic pockets of Cu-HHTC (3.9 Å) could barely fit the large electrolyte ions, thus lowering the electrochemically accessible surface area. In contrast, this is not the case for Cu-EP with its substantially larger intrinsic pockets (6.5 Å).

Besides, channel width and pocket size difference between the two MOFs also attributed to the capacitive performance. ³³ To gain further insights into distinguishing electrochemical properties with respect to the intrinsic pockets and channels, we conducted electrochemical impedance spectroscopy (EIS) analysis (Figure 4E). In the high-frequency region, the EIS plots show an incomplete semicircle, suggesting charge transport resistance. ^{34,35} Cu-EP resistance is comparable with Cu-HHTC, which corroborates their similar electrical conductivity. Both MOFs exhibit a linear Warburg impedance in the low-frequency region, suggesting an ion diffusion dominant process. ³⁶ We determined the Warburg coefficients of Cu-EP and Cu-HHTC to be 1,100 and 45,000, respectively, by plotting the Warburg impedance versus an inversed square root of angular frequency (Figure 4F). A smaller Warburg coefficient indicates a higher diffusion coefficient, ³⁷ thus corroborating the better diffusion of electrolytes in Cu-EP likely due to their substantially larger channels and pockets.

Post-synthetic metalation

Encouraged by the large intrinsic pockets in Cu-EP, we studied its possibility to host bulky ions, like Cs⁺. Although it can demonstrate size-exclusive host-guest interactions, we chose Cs ion because incorporation of Cs into the frameworks can provide access to additional functionalities, such as catalysis and light-emitting diodes, ^{38,39} where conducting platforms can be further advantageous. We investigated the size dependence on hosting Cs ion in contrast to the Li ion, distinguishing substantially different sizes (3.46 versus 1.42 Å)⁹ while both being alkali metal ions. Having different binding interactions expected between these ions and the pocket, we hypothesized that it might enable ion selectivity, further expanding potential applications of Cu-EP.⁴⁰ The post-synthetic metalation of Cu-EP was conducted using respective metal nitrate salts (2 equiv with respect to the EP ligand) to obtain metalated samples, namely Cu-EP-Li-2 and Cu-EP-Cs-2.

After metalation, the amounts of Li and Cs were quantified by XPS (Figures S26 and S27; Tables S6 and S7), which showed that no Li ions were detected while Cs occupancy was \sim 52% of the pockets. Cs(3d) XPS scan of the Cs-metalated framework clearly showed two distinct peaks at 724 and 738 eV, corresponding to $3d_{5/2}$ and $3d_{3/2}$, respectively. The binding energy of 724 eV suggests the oxidation state of Cs is +1.⁴¹ To further probe the ionic nature of Cs in the material, we conducted dye adsorption experiments, where either methylene blue (MB⁺) as a cationic dye or methyl orange (MO⁻) as an anionic dye can bind to the MOF depending on the overall charge of the material (Figure S29). The dye adsorption experiments





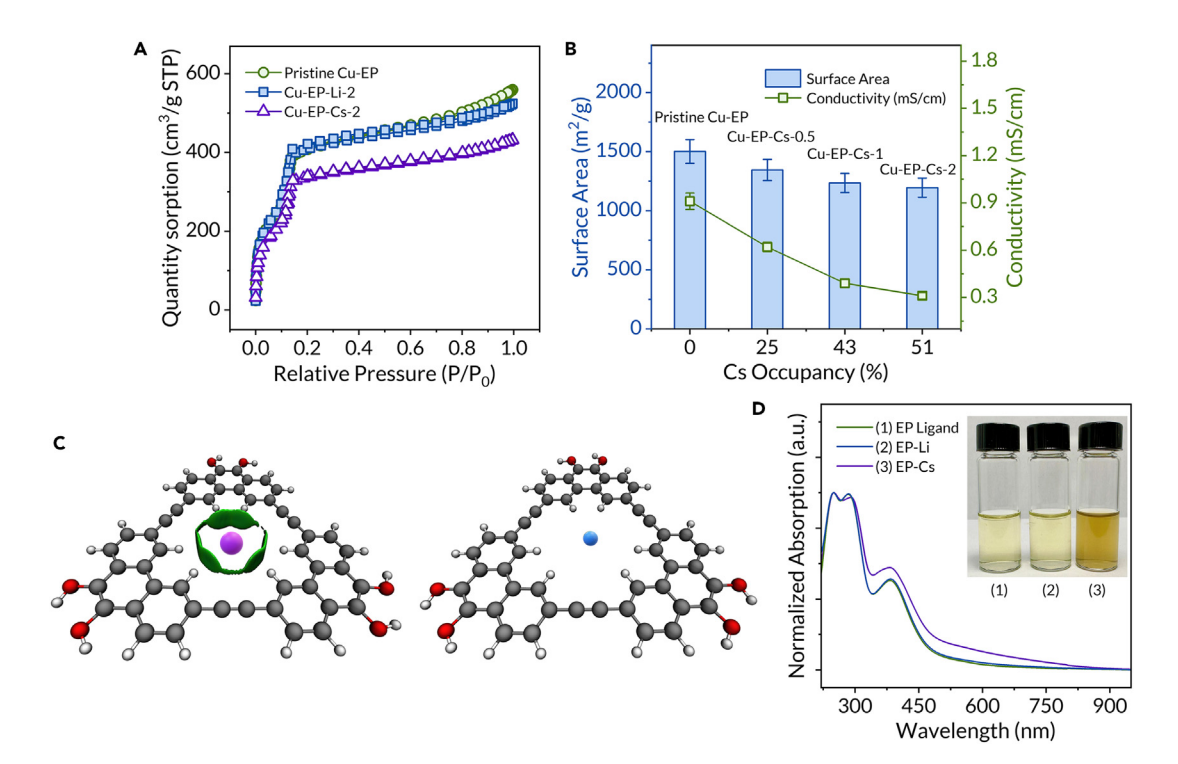


Figure 5. Post-synthetic metalation of Cu-EP and ion selectivity

- (A) Argon sorption isotherm of pristine Cu-EP, Cu-EP-Li-2, and Cu-EP-Cs-2.
- (B) Correlation between Cs occupancy with surface area and conductivity. Error bars represent standard deviation of surface area and electrical conductivity.
- (C) Independent gradient model based on Hirshfeld partition (IGMH) analysis of EP-Cs (left) and EP-Li (right) with isovalue $\delta g^{inter} = 0.001$ a.u. (gray: carbon, white: hydrogen, red: oxygen, purple: cesium, blue: lithium, and green: interaction region).
- (D) UV-vis-NIR absorption of free EP ligand, EP-Li, and EP-Cs complexes and their solutions (inset).

suggested that the pristine Cu-EP is likely negatively charged as it adsorbed the cationic MB⁺ significantly. After the Cs metalation, Cu-EP-Cs-2 exhibited a less negative character than the parent, implying the gain of positive charge characters due to Cs⁺ inclusion (Figure S29).

To confirm the inclusion of Cs in the framework, we collected PXRD after metalation. The experimental PXRD patterns show the retained crystallinity of the Cs-metalated sample, proving the intactness of the framework. Cu-EP-Cs-2 exhibited a new notable peak at $\sim\!5^\circ$, whereas Cu-EP-Li-2 showed no significant change upon metalation (Figure S30). To explain the structural change, we simulated structures where Cs ions are in the center of the pockets in [110] plane (in-plane) or sandwiched between adjacent planes with little offset (between-plane) (Figure S31). The in-plane structure closely matches the experimental diffraction patterns with the pronounced peak at $\sim\!5^\circ$, whereas the between-plane structure shows additional peaks at $\sim\!14.5^\circ$, which are absent in the experimental diffractions. Therefore, the Cs ion is more likely in the pocket (in-plane). Argon sorption at 77 K confirms that the isotherm and BET surface area of Cu-EP-Li-2 closely match the pristine Cu-EP, verifying the absence of Li in the framework. In contrast, Cu-EP-Cs-2 exhibits a lower quantity sorption and BET surface area than that of the pristine MOF, validating the occupancy of Cs (Figure 5A).

We also carried out a set of control experiments with the lowered salt concentrations from 2 to 1 and 0.5 equiv with respect to the EP ligand to vary metalation extent, namely Cu-EP-Cs-1 and Cu-EP-Cs-0.5. This control experiment aimed to test the





tunability and sensitivity of the metalation toward lower doses of Cs. Energy dispersive X-ray spectroscopy (EDS) determined that the pocket occupancy of Cu-EP-Cs-2, Cu-EP-Cs-1, and Cu-EP-Cs-0.5 shows gradual decreases as 51%, 43%, and 25%, respectively (Table S8) as the dosing amount decreased. EDS elemental mapping shows the homogeneous distribution of Cs (Figure S32). Measured BET surface areas of Cu-EP-Cs-2, Cu-EP-1, and Cu-EP-0.5 are closely aligned with their hypothetical surface areas upon metalation, confirming that Cs indeed occupied the pockets (Figure 5B; Table S10). The electrical conductivity moderately changed with varied Cs occupancies (Figure 5B), where the conductivity variations likely result from the modified electronic structures due to Cs insertion and oxidizing nature of the Cs salt (Table S11). These results suggest that controlling the material's pocket occupancy and the resulting properties should add another knob for controlling the MOF's properties.

Computational insights into ion selectivity

We employed computational studies to rationalize if the size difference of ions and their binding affinity to the pocket are the origin of the ion selectivity. The significant difference in ionic sizes of Li and Cs may induce different extents of binding affinity, influencing the thermodynamic stability of the metalated frameworks. To prove our hypothesis, we performed DFT calculations to measure binding energy between EP ligand with Li⁺ and Cs⁺ (Table S12). Our calculations indicated that the binding energy of Cs⁺ is larger than that of Li⁺ toward the EP ligand, suggesting a more stable EP-Cs complex than the Li counterpart. This result also supports that Cu-EP has a higher possibility to metalate Cs⁺ than Li⁺, corroborating the experimental trend. We further investigated the ion selectivity of the EP ligand using an independent gradient model based on Hirshfeld partition (IGMH) analysis. 43 IGMH can map the region of interaction at an isovalue δg^{inter} of 0.001 a.u., a threshold of interaction. As shown in Figure 5C, Cs interact strongly (green region) with the pocket, whereas it is absent in the Li case. We demonstrated the selectivity between Cs and Li ions by complexing them with free EP ligands. As shown in Figure 5D, the EP solution treated with Li salts showed no color change, whereas the EP-Cs complex readily intensified the solution color of the free EP ligand with a stronger absorption at 400 nm. This result corroborates the favored interaction between EP pocket and Cs⁺ in contrast to Li⁺, explaining the observed ion selectivity.

Conclusions

With design strategy in hand, we synthesized a macrocyclic ligand EP that possesses a large and functionalizable intrinsic pocket to tackle the low surface areas and the lack of diversity of functionalities in contemporary 2D EC-MOFs. With copper nodes, Cu-EP exhibits an electrical conductivity of 1.0 × 10⁻³ S/cm and a record-high surface area of 1,502 m²/g for the existing 2D EC-MOFs to date. The high surface area, large intrinsic pocket, and built-in redox activity of Cu-EP enhanced its capacitive performance. The sizable intrinsic pocket with the alkyne functional groups successfully demonstrated its capability to selectively host Cs⁺ over Li⁺. We believe that our work not only adds a new member to the series of macrocyclic ligand-based EC-MOFs but paves the way for expanding their possible applications where redox activity, ion selectivity, and high surface area are simultaneously desired.

EXPERIMENTAL PROCEDURES

Resource availability

Lead contact

Further information and requests for resources should be directed to and will be fulfilled by the lead contact, Jihye Park (jihye.park@colorado.edu).





Materials availability

This study did not generate new reagents.

Data and code availability

The data and code are available from the lead contact, Jihye Park upon reasonable request.

Materials and instrumentations

Chemicals were purchased from Sigma-Aldrich, Oakwood Chemical, or Fisher Scientific and used without any further purification. PXRD was taken using a Bruker D8 diffractometer with a copper beam source (λ = 1.5418 Å) at 40 kV and 40 mA. SEM was carried out on a field emission scanning electron microscope (JEOL JSM-7401F) at 5 kV. SEM EDS was conducted using Hitachi SU3500. TEM was carried out on Titan Themis GT 300 at 300 kV. Solution-phase UV-vis-NIR absorption spectra were recorded on a CARY 5000 spectrophotometer. To prepare the UV-vis-NIR sample, analytes were dispersed in a solution of methanol and water (20:1, v/v). Solid-phase infrared absorption spectra were recorded on a Cary 630 ATR FTIR spectrophotometer. Pore size, BET surface area, and argon sorption isotherms measurements were carried out with a Micromeritics ASAP 2020 PLUS porosimeter. Nuclear magnetic resonance (NMR) spectroscopy was performed on a Bruker AV-III 300 MHz spectrometer. XPS was measured by using a K-alpha spectrometer with an Al Kα X-ray source. Electrical conductivity was measured with a Keithley SCS-4200 parameter analyzer using the four-point probe method. Pressed pellets were prepared with approximately 5 mg of material in a 5 mm diameter circular dye under 1.5 Tons of pressure. Electrochemical characterizations were conducted on a Biologic VSP-300 instrument.

Synthesis of Cu-EP

EP ligand (10 mg, 0.0145 mmol) and $Cu(NO_3)_2 \cdot 2.5H_2O$ (5 mg, 0.0217 mmol) were added to a 20 mL vial charged with a stir bar, followed by 10 mL degassed DMF in an inert atmosphere. Then, 0.4 mL water was added to the vial. The solution was stirred at 60°C, 100 rpm, for 12 h. After that, the reaction was cooled to room temperature. The black solids were isolated by centrifugation, washed with DMF (2 × 10 mL), followed by acetone (2 × 10 mL). The product was then dried in a vacuum oven (20 mTorr) at 70°C for 1 h.

Electrochemical characterization

Cu-EP (75 wt %) was grounded with Super P (10 wt %) as the conducting additive and polytetrafluoroethylene (PTFE) (15 wt %). To the mixture, ethanol was added to obtain a homogeneous solution, which was drop-casted on the surface of the glassy carbon electrode before it was dried at 65°C for 15 min. CV was conducted using the modified glassy carbon electrode, Ag/Ag $^+$, and Pt wire as a working electrode, reference electrode, and counter electrode, respectively, in 1 M aqueous Na $_2$ CO $_3$ electrolyte with a scan rate of 10 mV/s. EIS was obtained at 0 V (versus Ag/Ag $^+$) by setting a set of alternating current (AC) signal of 10 mV to a frequency range of 1 MHz to 50 mHz.

Post-synthetic metalation of Cu-EP

Pristine Cu-EP (20 mg, 0.025 mmol ligand pocket) was added to a 20 mL vial. Then, corresponding LiNO $_3$ (2 equiv) or CsNO $_3$ 10 mM (2, 1, or 0.5 equiv) or CsOAc (2 equiv) in 10 mL methanol/water (20:1, v/v) was added to the vial. The mixture was standing at room temperature for 3 h. The solid was then isolated by centrifugation, washed with acetone twice (10 mL), and dried in a vacuum oven (20 mTorr) at 60°C for 1 h.

Chem



SUPPLEMENTAL INFORMATION

Supplemental information can be found online at https://doi.org/10.1016/j.chempr. 2023.08.026.

ACKNOWLEDGMENTS

J.P. acknowledges the start-up funds from the University of Colorado Boulder and the donors of the American Chemistry Society Petroleum Research Fund under grant no. 65505-DNI10. W.Z. thanks the National Science Foundation (CHE-2108197) for financial support. J.Y.C. acknowledges support from the Postdoctoral Fellowship from the National Research Foundation of Korea under grant no. NRF-2021R1A6A3A14044659. H.T.B.P. acknowledges support from the Graduate Research Fellowship Program from the National Science Foundation of the United States under grant no. DGE 2040434. We thank Benjamin Clayville for proofreading the manuscript.

AUTHOR CONTRIBUTIONS

H.T.B.P. and J.P. conceived and designed the experiments. H.T.B.P. performed most of the experiments. H.T.B.P. and J.P. analyzed the data. J.Y.C. acquired the TEM images and helped to revise the manuscript. X.F. performed the DFT calculations. A.C. helped with the synthesis. All authors were involved in the writing of the manuscript.

DECLARATION OF INTERESTS

The authors declare no competing interests.

INCLUSION AND DIVERSITY

One or more of the authors of this paper self-identifies as an underrepresented ethnic minority in field of research or within their geographical location. While citing references scientifically relevant for this work, we also actively worked to promote gender balance in our reference list.

Received: May 2, 2023 Revised: August 8, 2023 Accepted: August 28, 2023 Published: September 22, 2023

REFERENCES

- 1. Sheberla, D., Bachman, J.C., Elias, J.S., Sun, C.J., Shao-Horn, Y., and Dincă, M. (2017). Conductive MOF electrodes for stable supercapacitors with high areal capacitance. Nat. Mater. 16, 220-224.
- 2. Meng, Z., Aykanat, A., and Mirica, K.A. (2019). Welding metallophthalocyanines into bimetallic molecular meshes for ultrasensitive, low-power chemiresistive detection of gases. J. Am. Chem. Soc. 141, 2046-2053.
- 3. Liu, L., Xu, Q., and Zhu, Q.-L. (2021). Electrically conductive metal-organic frameworks for electrocatalytic applications. Adv. Energy Sustain. Res. 2, 2100100.
- 4. Thaggard, G.C., Haimerl, J., Fischer, R.A., Park, K.C., and Shustova, N.B. (2023). Traffic lights for catalysis: stimuli-responsive molecular and

- extended catalytic systems. Angew. Chem. Int. Ed. Engl. 62, e202302859.
- 5. Stanley, P.M., Haimerl, J., Shustova, N.B., Fischer, R.A., and Warnan, J. (2022). Merging molecular catalysts and metal-organic frameworks for photocatalytic fuel production. Nat. Chem. 14, 1342-1356.
- 6. Xie, L.S., Skorupskii, G., and Dincă, M. (2020). Electrically conductive metal-organic frameworks. Chem. Rev. 120, 8536-8580.
- 7. Zhang, Z., Valente, D.S., Shi, Y., Limbu, D.K., Momeni, M.R., and Shakib, F.A. (2023). In silico high-throughput design and prediction of structural and electronic properties of lowdimensional metal-organic frameworks. ACS Appl. Mater. Interfaces 15, 9494-9507.
- 8. Pham, H.T.B., Choi, J.Y., Huang, S., Wang, X., Claman, A., Stodolka, M., Yazdi, S., Sharma, S., Zhang, W., and Park, J. (2022). Imparting functionality and enhanced surface area to a 2D electrically conductive MOF via macrocyclic linker. J. Am. Chem. Soc. 144, 10615-10621.
- 9. Kuma, K., Usui, A., Paplawsky, W., Gedulin, B., and Arrhenius, G. (1994). Crystal structures of synthetic 7 angstrom and 10 angstrom manganates substituted by mono- and divalent cations. Mineral. Mag. 58, 425-447.
- 10. Wang, X., Ramírez, P.J., Liao, W., Rodriguez, J.A., and Liu, P. (2021). Cesium-induced active sites for C-C coupling and ethanol synthesis from CO₂ hydrogenation on Cu/ ZnO(0001) surfaces. J. Am. Chem. Soc. 143, 13103-13112.





- Liu, X., Chen, M., Zhang, Y., Xia, J., Yin, J., Li, M., Brooks, K.G., Hu, R., Gao, X., Kim, Y.-H., et al. (2022). High-efficiency perovskite photovoltaic modules achieved via cesium doping. Chem. Eng. J. 431, 133713.
- Nightingale, E.R., Jr. (1959). Phenomenological theory of ion solvation. Effective radii of hydrated ions. J. Phys. Chem. 63, 1381–1387.
- 13. Zhang, L., Yang, X., Zhang, F., Long, G., Zhang, T., Leng, K., Zhang, Y., Huang, Y., Ma, Y., Zhang, M., et al. (2013). Controlling the effective surface area and pore size distribution of sp² carbon materials and their impact on the capacitance performance of these materials. J. Am. Chem. Soc. 135, 5921–5929.
- Montoya Sánchez, N., and de Klerk, A. (2018). Autoxidation of aromatics. Appl. Petrochem. Res. 8, 55–78.
- D'Alessandro, D.M. (2016). Exploiting redox activity in metal-organic frameworks: concepts, trends and perspectives. Chem. Commun. (Camb) 52, 8957–8971.
- Thaggard, G.C., Haimerl, J., Park, K.C., Lim, J., Fischer, R.A., Maldeni Kankanamalage, B.K.P., Yarbrough, B.J., Wilson, G.R., and Shustova, N.B. (2022). Metal–photoswitch friendship: from photochromic complexes to functional materials. J. Am. Chem. Soc. 144, 23249–23263.
- Martin, C.R., Park, K.C., Leith, G.A., Yu, J., Mathur, A., Wilson, G.R., Gange, G.B., Barth, E.L., Ly, R.T., Manley, O.M., et al. (2022). Stimuli-modulated metal oxidation states in photochromic MOFs. J. Am. Chem. Soc. 144, 4457–4468.
- Cui, S., Huang, Q., Wang, J., Jia, H., Huang, P., Wang, S., and Du, P. (2019). From planar macrocycle to cylindrical molecule: synthesis and properties of a phenanthrene-based coronal nanohoop as a segment of [6,6]carbon nanotube. Org. Lett. 21, 5917–5921.
- Phulwale, B.V., Mishra, S.K., and Mazal, C. (2018). Synthesis and properties of π-conjugated donor-acceptor macrocycles derived from phenanthrylene building blocks. Tetrahedron 74, 3616–3623.
- He, Z., Xu, X., Zheng, X., Ming, T., and Miao, Q. (2013). Conjugated macrocycles of phenanthrene: a new segment of [6,6]-carbon nanotube and solution-processed organic semiconductors. Chem. Sci. 4, 4525.
- Yang, H., Du, Y., Wan, S., Trahan, G.D., Jin, Y., and Zhang, W. (2015). Mesoporous 2D covalent organic frameworks based on shape-persistent arylene-ethynylene macrocycles. Chem. Sci. 6, 4049–4053.
- Bordwell, F.G., McCallum, R.J., and Olmstead, W.N. (1984). Acidities and hydrogen bonding of phenols in dimethyl sulfoxide. J. Org. Chem. 49, 1424–1427.

- Olmstead, W.N., Margolin, Z., and Bordwell, F.G. (1980). Acidities of water and simple alcohols in dimethyl sulfoxide solution. J. Org Chem. 45, 3295–3299.
- Dou, J.H., Arguilla, M.Q., Luo, Y., Li, J., Zhang, W., Sun, L., Mancuso, J.L., Yang, L., Chen, T., Parent, L.R., et al. (2021). Atomically precise single-crystal structures of electrically conducting 2D metal-organic frameworks. Nat. Mater. 20, 222–228.
- Dou, J.H., Sun, L., Ge, Y., Li, W., Hendon, C.H., Li, J., Gul, S., Yano, J., Stach, E.A., and Dincă, M. (2017). Signature of metallic behavior in the metal-organic frameworks M₃ (hexaiminobenzene)₂ (M = Ni, Cu). J. Am. Chem. Soc. 139, 13608-13611.
- Li, W.-H., Ding, K., Tian, H.-R., Yao, M.-S., Nath, B., Deng, W.-H., Wang, Y., and Xu, G. (2017). Conductive metal-organic framework nanowire array electrodes for highperformance solid-state supercapacitors. Adv. Funct. Mater. 27, 1702067.
- Chen, T., Dou, J.H., Yang, L., Sun, C., Libretto, N.J., Skorupskii, G., Miller, J.T., and Dincă, M. (2020). Continuous electrical conductivity variation in M₃ (hexaiminotriphenylene)₂ (M = Co, Ni, Cu) MOF alloys. J. Am. Chem. Soc. 142, 12367–12373.
- Yao, M.S., Zheng, J.J., Wu, A.Q., Xu, G., Nagarkar, S.S., Zhang, G., Tsujimoto, M., Sakaki, S., Horike, S., Otake, K., et al. (2020). A dual-ligand porous coordination polymer chemiresistor with modulated conductivity and porosity. Angew. Chem. Int. Ed. Engl. 59, 172–176.
- Park, J., Hinckley, A.C., Huang, Z., Feng, D., Yakovenko, A.A., Lee, M., Chen, S., Zou, X., and Bao, Z. (2018). Synthetic routes for a 2D semiconductive copper hexahydroxybenzene metal-organic framework. J. Am. Chem. Soc. 140, 14533–14537.
- Nagatomi, H., Yanai, N., Yamada, T., Shiraishi, K., and Kimizuka, N. (2018). Synthesis and electric properties of a two-dimensional metalorganic framework based on phthalocyanine. Chemistry 24, 1806–1810.
- de Lourdes Gonzalez-Juarez, M., Morales, C., Flege, J.I., Flores, E., Martin-Gonzalez, M., Nandhakumar, I., and Bradshaw, D. (2022).
 Tunable carrier type of a semiconducting 2D metal-organic framework Cu₃(HHTP)₂. ACS Appl. Mater. Interfaces 14, 12404–12411.
- 32. Feng, D., Lei, T., Lukatskaya, M.R., Park, J., Huang, Z., Lee, M., Shaw, L., Chen, S., Yakovenko, A.A., Kulkarni, A., et al. (2018). Robust and conductive two-dimensional metal—organic frameworks with exceptionally high volumetric and areal capacitance. Nat. Energy 3, 30–36.

- Izadi-Najafabadi, A., Futaba, D.N., Iijima, S., and Hata, K. (2010). Ion diffusion and electrochemical capacitance in aligned and packed single-walled carbon nanotubes.
 J. Am. Chem. Soc. 132, 18017–18019.
- Stodolka, M., Choi, J.Y., Flood, J., Pham, H.T.B., and Park, J. (2022). Iron-based 2D conductive metal-organic framework nanostructure with enhanced pseudocapacitance. ACS Appl. Nano Mater. 5, 2156–2162.
- 35. Shinde, S.S., Lee, C.H., Jung, J.-Y., Wagh, N.K., Kim, S.-H., Kim, D.-H., Lin, C., Lee, S.U., and Lee, J.-H. (2019). Unveiling dual-linkage 3D hexaiminobenzene metal-organic frameworks towards long-lasting advanced reversible Znair batteries. Energy Environ. Sci. 12, 727–738.
- Choi, J.Y., Flood, J., Stodolka, M., Pham, H.T.B., and Park, J. (2022). From 2D to 3D: postsynthetic pillar insertion in electrically conductive MOF. ACS Nano 16, 3145–3151.
- Lasia, A. (2002). Electrochemical impedance spectroscopy and its applications. In Modern Aspects of Electrochemistry Modern Aspects of Electrochemistry, B.E. Conway, J.O. Bockris, and R.E. White, eds. (Springer), pp. 143–248.
- Li, Y., Lou, Y.-H., Zhou, Y.-H., Xia, Y., Wang, B., and Wang, Z.-K. (2023). Review on the promising roles of alkali metals toward highly efficient perovskite light-emitting diodes. J. Mater. Chem. C 11, 2011–2025.
- Wang, Y., Liu, K., Wu, J., Hu, Z., Huang, L., Zhou, J., Ishihara, T., and Guo, L. (2020). Unveiling the effects of alkali metal ions intercalated in layered MnO₂ for formaldehyde catalytic oxidation. ACS Catal. 10, 10021– 10031.
- 40. Lu, J., Hu, X., Ung, K.M., Zhu, Y., Zhang, X., and Wang, H. (2022). Metal–organic frameworks as a subnanometer platform for ion–ion selectivity. Acc. Mater. Res. 3, 735–747.
- Morgan, W.E., Van Wazer, J.R., and Stec, W.J. (1973). Inner-orbital photoelectron spectroscopy of the alkali metal halides, perchlorates, phosphates, and pyrophosphates. J. Am. Chem. Soc. 95, 751-755.
- Choi, J.Y., Stodolka, M., Kim, N., Pham, H.T.B., Check, B., and Park, J. (2023). 2D conjugated metal-organic framework as a proton-electron dual conductor. Chem 9, 143–153.
- Lu, T., and Chen, Q. (2022). Independent gradient model based on Hirshfeld partition: a new method for visual study of interactions in chemical systems. J. Comput. Chem. 43, 539–555.